Band structure and optical properties of ordered $AuCu_3$

H. L. Skriver* and H. P. Lengkeek
Kamerlingh Onnes Laboratory der Rijksuniversiteit Leiden, The Netherlands
(Received 15 June 1977)

The optical spectra of ordered $AuCu_3$ have been measured at low temperatures by a direct ellipsometric technique. We find several structural elements above the absorption edge as well as in the infrared. The measured spectra are interpreted in terms of the interband absorption calculated from an *ab initio* band structure obtained by the relativistic linear muffin-tin orbitals method. The band calculation reveals that ordered $AuCu_3$ has distinct copper and gold d bands positioned in and hybridizing with an s band common to copper and gold. The calculated state density is found to be in good agreement with experiment. The Fermi surface is presented and is found to originate mainly in copper $4s$ and $4p$ states.

I. INTRODUCTION

The copper-gold system has a continuous range of solid solubility and includes several compounds, some of which may be prepared both in an ordered and a disordered state. It has therefore for many years been recognized[1-3] as ideal for the study of order-disorder transformations in alloys. Recent experiments on the copper-rich compound $AuCu_3$ include studies of the change of the specific heat,[4,5] the optical properties,[6-10] and the x-ray photoelectron spectra[11] on ordering.

The effect of the order-disorder transformation on the electronic specific heat is found to be small, suggesting little change in the density of states at the Fermi level. Similarly, although new optical transitions are introduced on ordering, the effect is only of the order of 10%, indicating moderate changes of the band structure away from the Fermi energy. Nilsson and Norris[8] interpreted the change in the optical absorption in terms of energy gaps opened by new Bragg reflection planes, while Scott and Muldawer[10] suggested that a folding of the energy bands might be responsible.

The measured optical spectra disagree somewhat as to the exact position of some of the structure observed, but show qualitative resemblance with the spectra of pure copper and gold, and may tentatively be interpreted in terms of the available energy bands for the pure elements. In addition to the copper- and gold-like structure in the range above 2 eV, Scott and Muldawer[10] found a pronounced maximum at 1.3 eV which has no obvious explanation in terms of the band structures of copper and gold, or the existing energy bands[12] of $AuCu_3$.

From a theoretical point of view, the ordered $AuCu_3$ phase is interesting because it represents one point in the range from pure copper to pure gold, which is accessible to band-structure calculations. This is more so since, while the theory of energy bands of disordered alloys is still in its infancy, the recent formulation of the band theory[13] for ordered closely packed systems has proven so fast and accurate that four atoms per unit cell even with relativistic corrections represent no computational difficulties. This may be appreciated by noting that the present work includes five full-scale band calculations.

The present study was undertaken in order to establish an interpretation of the available optical measurements on ordered $AuCu_3$ in terms of first-principles energy bands. We have employed the relativistic linear muffin-tin orbitals (LMTO) method[13,14] in conjunction with a non-self-consistent potential, and have calculated the optical spectra assuming constant dipole-matrix elements. Since the previous optical measurements gave differing spectra we decided to remeasure the optical constants of ordered $AuCu_3$ by a direct and accurate technique which avoids Kramers-Kronig analysis. As the calculations suggested transitions in the infrared, the experiments were performed at low temperature in order to reduce the Drude contribution which otherwise would mask the low-energy transitions.

The organization of the paper is as follows. In Sec. II we briefly mention concepts entering the LMTO method, and estimate the errors in the various steps of the present calculations. Section III contains the experimental procedures, and a presentation of the optical spectra obtained. In Sec. IV we present the energy bands, the state density, and the Fermi surface. Finally, in Sec. V we present the calculated optical properties, and compare with measurements, thereby obtaining an interpretation of experimental spectra.

II. METHOD OF CALCULATION

Since the LMTO method is thoroughly described elsewhere,[13] and since the details of the present version of the calculations may be found in Refs. 15 and 16, we will only briefly mention the main

features of the technique. The method combines some of the most desirable properties of the Korringa-Kohn-Rostoker (KKR) and the linear combination of atomic orbitals (LCAO) methods. Like the KKR method it has the capability to treat accurately both simple and d-band metals. At the same time the method is computationally fast since the secular equations are of the LCAO form, i.e., they reduce to eigenvalue equations from which all the eigenvalues and eigenvectors for a given Bloch vector may be obtained in one single diagonalization.

Within the atomic-sphere approximation[13] the LMTO method is separated into two distinct parts, one of which depends only on the crystal potential and the volumes of the atomic spheres and which is expressed by potential parameters, and the other depending solely on the crystal structure and which is expressed by canonical structure constants. We will now discuss the potential dependent and the structure dependent parts separately.

A. Potential and potential parameters

The crystal potential enters the LMTO method via the logarithmic derivative function $D_l(E) = S\phi_l(E,S)/\phi_l'(E,S)$ derived from the potential and evaluated at the atomic radius S. Here $\phi_l(E,S)$ is the radial wave function normalized to unity in the atomic sphere. It is shown by Andersen[13,14] that only four independent parameters $D_{\nu l}$, a_l, b_l, and m_l are needed to describe accurately the logarithmic derivative functions $D_l(E)$ in the energy range of interest for band calculations. This is achieved in the absence of spin-orbit interaction by the truncated Laurent expansion

$$[D_l(E) - D_{\nu l}]^{-1} = [m_l S^2(E - E_{\nu l})]^{-1} + a_l + b_l S^2(E - E_{\nu l}), \tag{1}$$

where $E_{\nu l}$ is an arbitrary energy around which the expansion is made, and $D_{\nu l}$ is the logarithmic derivative at $E_{\nu l}$. By solving the Dirac equation rather than the Schrödinger equation, one may include the mass-velocity and Darwin corrections in the parameters, and further obtain the spin-orbit parameters ξ_l and $\omega_l(D^l)$ describing the spin-orbit splitting at $D_{\nu l}$ and its D dependence.

The significance of these parameters may be appreciated if we note that for a given boundary condition, e.g., $D_{\nu l} = -l-1$, a_l, b_l, and m_l vary only slowly as we move along for instance the $4d$ series of the periodic table. The parameters may furthermore be combined to obtain physically more significant parameters. If we make the above choice of $D_{\nu l} = -l-1$, the corresponding $E_{\nu l}$ will be the center $c_{\nu l}$ of the νl band and we may obtain the intrinsic band mass $\mu_l = 2m_l(c_{\nu l})$, which is inversely proportional to the width of the νl band. Further evidence of the physical significance of the LMTO potential parameters may be found in Refs. 13, 15, and 16.

The spherically symmetric part of the muffin-tin potential was constructed by superimposing relativistic Dirac-Slater self-consistent atomic charge densities for the neutral atoms. Exchange and correlation were included throughout by the Slater $\rho^{1/3}$ approximation with $\alpha = 1$. This construction does not take charge transfer fully into account, and this is expected to be the main source of uncertainty in the present results. However, calculations with an equivalent potential on β'-MgHg,[16] β'-brasses,[17] and $^{15}Pt_3Sn$ give Fermi surfaces and optical properties in good agreement with experiment. This indicates that the electron density in the above construction is physically reasonable for closely packed metallic systems, and that the neglect of an explicit charge transfer may not lead to appreciable errors in the band structure. The relevant crystal potential data are listed in Table I. The parameters used in the band calculations are shown in Table II. We have chosen to use central parameters, i.e., taken $E_{\nu l}$ to be equal to the center $C_{\nu l}$ of the νl band defined by $D_l(C_{\nu l}) = -l-1$ since this choice gives the best overall energy bands.

In the actual calculations we have included also the corrections[13] to the atomic sphere approximation which re-establish the interstitial region and improve the l convergence. From Eq. (4.24) of Ref. 13 we estimate the maximum error of our procedure to be 0.11, 0.20, and 0.07 eV at the Fermi level for the Cu $4s$, $4p$, and Au $6s$ states, respectively.

B. Canonical and unhybridized bands

The crystal structure enters the LMTO method via structure constants which are canonical in the sense that they depend neither on energy nor on the scale of the lattice. By diagonalization of the ap-

TABLE I. Crystal potential data for Au and Cu in $AuCu_3$, and for Cu_4. The table gives the lattice spacing a, the atomic configuration, the muffin-tin zero E_{MTZ}, the muffin-tin radii S_{MT}, and the discontinuity Δ_{MT} at the muffin-tin sphere.

	Au		Cu	Cu_4
a (A)		3.748		3.748
Configuration	$5d^{10}6s$		$3d^{10}4s$	$3d^{10}4s$
E_{MTZ} (Ry)		−1.1617		−1.103
S_{MT} (a.u.)	2.586		2.340	2.460
Δ_{MT} (mRy)	162.0		90.0	80.0

TABLE II. Potential parameters for Au and Cu as used in the band calculations. The relativistic parameters contain the mass-velocity and Darwin corrections, while the nonrelativistic do not. S is the radius of a sphere that has $\frac{1}{4}$ of the volume of the unit cell. With the boundary conditions $D_l(E_\nu) = -l-1$ the four parameters $E_\nu = C$, $m(C) = \frac{1}{2}\mu$, a and b are used to describe the logarithmic derivative function $D_l(E)$ through Eq. (1). The parameters ξ and $\omega(D^l)$ give the spin-orbit splitting at E_ν and its D dependence (or implicitly its energy dependence) in the l-band region. The remaining parameters give in dimensionless units the relative position of the p and d bands with respect to the s band. The free-electron values (Ref. 13) for C_{ps} and C_{ds} are 7.4 and 17.7, respectively.

		Au		Cu		Cu_4
		Relativistic	Nonrelativistic	Relativistic	Nonrelativistic	Relativistic
S (a.u.)		2.9747	2.9747	2.6917	2.6917	2.7679
	s	0.113	0.404	0.293	0.323	0.229
$E_\nu = C$(Ry)	p	1.122	1.309	1.242	1.259	1.128
above E_{MTZ}	d	0.203	0.338	0.343	0.361	0.278
	s	0.879	0.730	0.863	0.846	0.889
$\mu = 2m(C)$	p	0.890	0.820	0.994	0.985	1.016
	d	7.362	6.176	18.032	17.570	19.570
	s	0.160	0.142	0.164	0.161	0.166
a	p	0.132	0.125	0.144	0.143	0.146
	d	0.181	0.182	0.205	0.205	0.204
	s	0.268	0.198	0.297	0.287	0.311
$100\,b$	p	0.172	0.153	0.226	0.222	0.232
	d	0.431	0.433	0.640	0.644	0.631
ξ(mRy)	p	148.2		15.4		14.2
	d	49.9		9.0		9.0
$\omega(D^l)$ (Ry)	p	−4.21		−3.73		−3.36
	d	−1.50		−1.32		−1.25
$C_{ps} = (C_p - C_s)S^2$		8.93	8.00	6.88	6.78	6.87
$C_{ds} = (C_d - C_s)S^2$		0.80	−0.58	0.36	0.28	0.38

propriate submatrices of the structure constant matrix one obtains the canonical s, p, and d bands for each type of atom. These bands have the dispersion of real energy bands, and contain all the structural information needed to form a real band structure. Within the atomic sphere approximation, and using the boundary condition $D_{\nu l} = -l-1$, one then derives the unhybridized l band of type t by placing the corresponding canonical band at C_{tl}, scaling it by $\mu_{tl} \equiv 2m_{tl}(C_{tl})$ and distorting it by a_{tl} and b_{tl}. This approximate description which is obtained at very low computational costs will eventually be used to establish the origin of the various features of the full-energy band calculations.

C. State-density calculations and optical spectra

The number of states $n(E)$, the density of states $N(E)$, and the joint density of states $J(\omega)$ are derived from the first-principles eigenvalues at 286 k's in the irreducible zone by the tetrahedron technique.[18] The calculated imaginary part $\epsilon_2(\omega) \sim J(\omega)/\omega^2$ of the dielectric constant consists of contributions from 91 band pairs which should be compared to the 6 which contribute in pure copper. The limited number of k points is estimated to give an error of less than 0.2 eV in the location of prominent structure. We further neglect the variation of the optical-matrix elements, which may account for the differences in amplitude between the calculated and the measured spectra. Judging from the results on pure copper[19] we might expect that the inclusion of matrix elements would turn the shoulder at 2.5 eV in our calculated $AuCu_3$ spectrum into a peak, giving a reasonably faithful interpretation of the measured $\epsilon_2(\omega)$ spectrum in terms of the calculated $J(\omega)/\omega^2$.

III. EXPERIMENTAL PROCEDURE

A. Sample preparation

A polycrystalline $AuCu_3$ sample (component purity: 5N+; crystal dimension: ~2 mm) was cut and planed by spark erosion into its final disk shape (diameter: 27 mm; thickness: 3 mm). Attempts to electropolish the sample failed, because of preferential etching of the crystallites, and therefore the surface was prepared by standard mechanical-polishing techniques. The sample was ordered by an anneal in vacuum ($< 10^{-6}$ Torr) for 70 h at 360 °C and slow cooling for 8 h. Separate x-ray diffraction experiments[20] on the ordering of

$AuCu_3$ samples (powdered) as a function of anneal temperature and time indicate an ordering of at least 96% for the optical sample. Addition effects of the heat treatment which were observed are the appearance of some relief structure and a cleaning of the surface,[21] indicated by the thermal etching. After mounting in the cryostat, the sample was annealed in vacuum for 5 h at 200 °C directly before measurement.

B. Optical measurement

The optical properties were measured between 0.5 and 5.3 eV at 30 K, using a Beattie system (angle of incidence $\simeq 69°$) described elsewhere.[22,23] The setup was improved over that described in Ref. 22 by the use of an Ortholoc, model 9502 lock-in amplifier, which has a relative high stability of the output signal. We furthermore used one photomultiplier (E.M.I. 9798 QB) instead of two for the energy range from 1.4 to 5.3 eV, thereby reducing difficulties with changing detectors. The low temperatures were obtained by use of a semiflow cryostat with a copper botton on which a sample holder (copper) could be mounted. A heater, mounted on the copper end, and fed by a temperature controller, served to stabilize the temperature in the range from 20 to 1000 K. The temperature was measured by a Au–0.3-at.%–Fe versus chromel thermocouple.

At high temperatures (600 K) and low pressure (10^{-7} Torr) the evaporation of the copper parts is considerable. Therefore, we screened the copper surfaces by means of an electrochemically deposited layer of ruthenium (approximately 1 μ thick). Ruthenium is very suitable for this purpose, because it hardly dissolves in copper, even at high temperatures. Since the sample, when it is at 30 K, acts as a cryopump, and therefore will be covered with an unwanted surface layer, it has to be shielded from the rest of the "vacuum" space. Here we used a thin (100 μm) copper shield, which surrounded the sample as closely as possible, with a small entrance and exit hole for the passage of the light beam. Both sample and shield were kept at 30 K.

The following procedure was employed to clean the sample from surface layers at low temperature: a cooling to 30 K in approximately 10 min. By measuring the absorption during these steps, it was established that a layer had formed at 30 K, which disappeared at high temperature. After the cleaning, tests showed that a new layer, which could influence the optical properties of the pure sample considerably, was not formed on the time scale of the total measurements (7 h). At this stage the vacuum was better than 10^{-7} Torr. An extensive error analysis of the setup and our measuring procedure is given in Ref. 23.

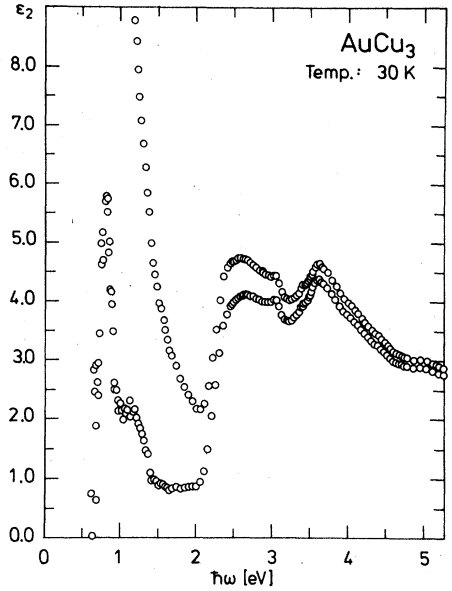

FIG. 1. Measured absorption $\epsilon_2(\omega)$ at 30 K (upper curve) and $\epsilon_2(\omega)$ corrected for intraband contributions (lower curve).

IV. MEASURED SPECTRA

Our results for the optical constants of ordered $AuCu_3$ are presented in Figs. 1–3. The $\epsilon_2(\omega)$ spectrum of Fig. 1 shows the following salient structures: maxima at 2.6 and 3.0 eV, a strong inflection point at 3.4 eV, a peak at 3.6 eV and a maximum at 5.0 eV. Weaker structure is discernable

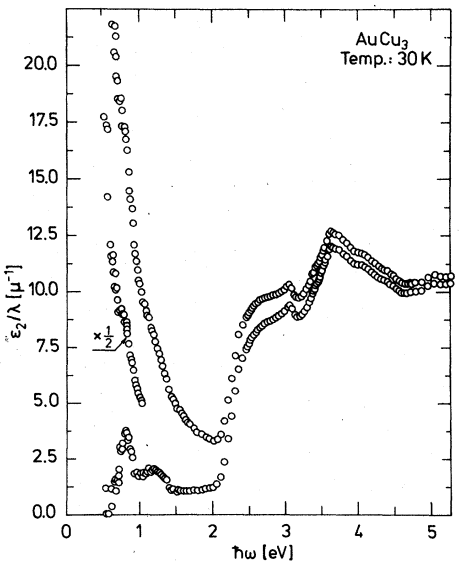

FIG. 2. Measured ϵ_2/λ spectrum at 30 K (upper curve) and ϵ_2/λ corrected for intraband contributions (lower curve).

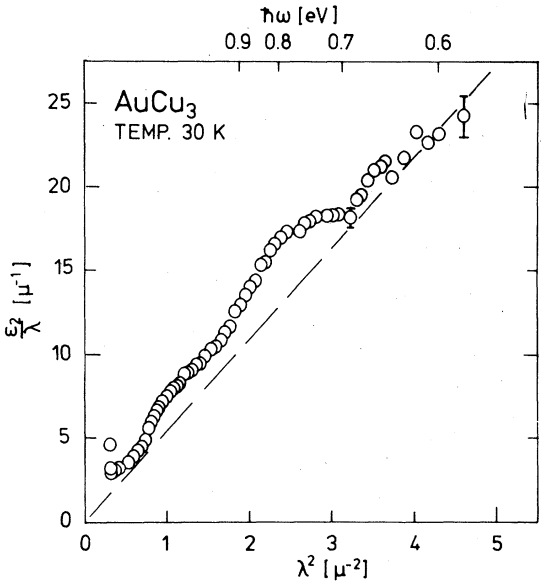

FIG. 3. ϵ_2/λ spectrum plotted against λ^2 showing the interband absorption in the infrared. The straight line corresponds to the intraband correction of Eq. (1).

[especially in the plots of $\epsilon_2(\omega)\lambda$, Figs. 2 and 3] in the infrared between 0.7 and 1.5 eV and in the ultraviolet at 4.1 and 4.4 eV.

To elucidate the structure in the infrared we attempt to subtract the intraband contribution using the simple model proposed by Lenham[24]

$$\epsilon_2(\omega)/\lambda = A\lambda^{\alpha} + B,$$

with $B=0$, and $\alpha=2$, following Drude theory. The value of $A \approx 5.5$ (μm^{-3}) was estimated from the plot of ϵ_2/λ versus λ^2, Fig. 3. This value is, in view of the deviation of $\epsilon_2(\omega)/\lambda$ from the Drude theory, not reliable enough to derive significant values of the intraband parameters. Also, values of ϵ_2 are very different for various workers,[6-10] indicating an influence of surface treatment and measurement conditions (vacuum).

The results of subtracting the intraband contribution are presented in Figs. 1 and 2. The structure that emerges clearly is a substantial contribution at 0.8 eV and a shoulder at 1.2 eV. Further evidence for these features may be found in the Drude plot Fig. 3, and in a plot of the reflection R versus energy, where the 0.8-eV contribution shows up as a 1% reduction in R. It should be noted that the structure in the infrared cannot be attributed to the excitation of surface plasmons as, in this photon energy range, $\epsilon_1(\omega)$ is of order 85. Comparing with other workers we find that our $\epsilon_2(\omega)$ spectrum is similar to, but has additional and sharper features than those of Nilsson and Norris[8] and Rivory,[9] and it is markedly different from that of Scott and Muldawer.[10] The latter authors neglected to compare their results with the earlier extensive direct measurements of Stahl *et al.*,[7] with which we find excellent agreement. Again, however, we obtain a more detailed spectrum, presumably as a result of the low temperature, the improved accuracy, and the high degree of long-range order in our sample. Scott and Muldawer[10] find pronounced structure in the range from 1 to 2 eV, and their peak at 1.3 eV may be compared to our contribution at 1.2 eV. Unfortunately however, since Scott and Muldawer were mainly looking at the order-disorder effects in the ultraviolet, the accuracy of their Fig. 2 in the 1–2 eV range is too small to make a comparison really meaningful.

V. ENERGY BANDS

The relativistic energy bands of ordered $AuCu_3$ as calculated by the LMTO method including spin-orbit interaction are shown in Fig. 4. The analysis in terms of the canonical bands of the $AuCu_3$ structure shows that they consist of distinct Au 5*d*, and Cu 3*d* bands hybridizing with Au 6*s* and Cu 4*s* states, and of a common conduction band formed by Au 6*s* as well as Cu 4*s* and 4*p* states. The bands are filled to well above the Cu 3*d* band, and the Fermi level crosses band numbers 22, 23, and 24.

Since the bands near the symmetry point M and close to the Fermi level prove to be important for the calculated optical properties of $AuCu_3$ in the infrared, we have collected in Fig. 5 the results of five band calculations along the symmetry line T. It is then possible to visualize the synthesis of the hybridized bands by comparing them with the unhybridized results.

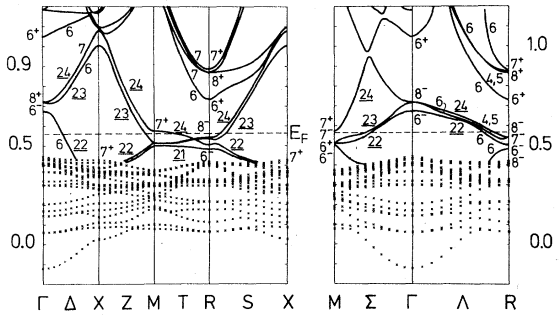

FIG. 4. Relativistic energy bands for ordered $AuCu_3$ obtained by the LMTO method, and plotted along the symmetry lines. The important bands are indexed (shown as underlined numbers) according to the convection $E_{j+1} > E_j$, and labeled in double group notation.

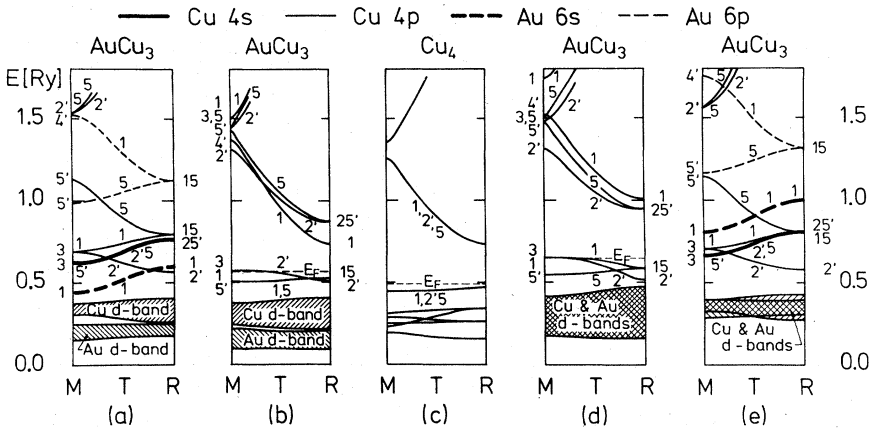

FIG. 5. Comparison of several band models for $AuCu_3$ calculated from the potential parameters of Table II: (a): unhybridized bands with relativistic corrections; (b): hybridized relativistic bands corresponding to the bands of Fig. 5 without spin-orbit splitting; (c): relativistic bands of Cu_4 without spin-orbit splitting; (d): hybridized nonrelativistic bands; and (e): unhybridized nonrelativistic band.

Comparing panels (a) and (b) of Fig. 5 we find that the T_2' level arises mainly as the result of strong hybridization between the bonding Cu $4p$ states and the antibonding Cu $4s$ states. Similarly, we find that the T_5 level is mainly a result of hybridization between Cu $4s$, Cu $4p$, and lower-lying (not shown) Cu $3d$ states. These two conclusions also hold true for the bands without mass-velocity and Darwin corrections, panels (d) and (e).

Turning again to panels (a) and (b) it appears that the T_1 level which is almost degenerate with the T_5 level is mainly of antibonding Au $6s$ character although it is shaped somewhat by weak hybridization with Cu $4p$ and lower-lying Cu $3d$ states. Comparing panels (a) and (e) however, we find that owing to the rise of the Au $6s$ band when the mass-velocity and Darwin corrections are omitted, the T_1 level in this case is mainly of Cu $4p$ character. In terms of the bands of fcc copper folded into the simple cubic Brillouin zone, named Cu_4 and shown in panel (c), we would say that the bands along T are due to a crystal potential splitting of the fourfold degenerate T_1, T_2', T_5 levels.

As a final point we may note that the mass-velocity and Darwin corrections separate the Cu $3d$ and the Au $5d$ bands although they still have an indirect overlap. This is in contrast to the case of low-concentration AuCu alloys where Beaglehole and Earlbach[1] found that one common d band was formed out of the copper and gold d states.

If we compare the present energy bands with the previous calculation of Gray and Brown[12] we find that their band structure is qualitatively similar, as expected, to our results without the relativistic effects. However, there are large quantitative differences. The width of their d bands is 4.5 eV, and the top of their Cu d bands falls at 3.7 eV below the Fermi level. This is 1 eV narrower and 1.7 eV lower than the present results and the two models will therefore lead to rather different optical properties.

A. State density

The density of states and the number of states functions derived from the bands in Fig. 4 are shown in Fig. 6. The top of the Cu $3d$ band is found at 0.13 Ry, i.e., 1.8 eV below the Fermi level. This is in good agreement with the x-ray photoelectron spectrum[11] also shown in Fig. 6, and with the electron distribution curves given by Nilsson and Norris.[8] In contrast, the calculated Au $5d$ band seems to be positioned 0.4 eV too low. However, if we shift the Au $5d$ band upwards, and take the experimental broadening into account, the agreement with the x-ray photoelectron spectrum is remarkably good. In Table III we have collected values of the density of states at the Fermi level $N(E_F)$ for several band models. The fact that, among the results for ordered $AuCu_3$, the relativistic calcula-

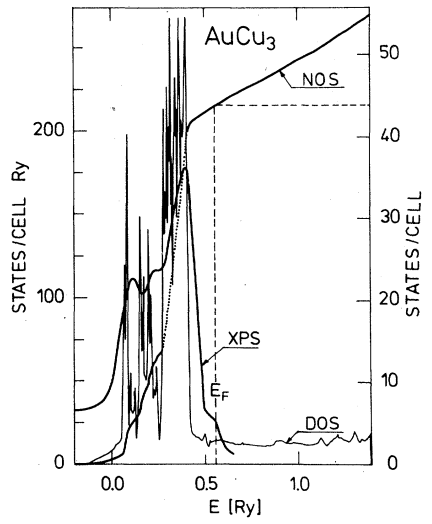

FIG. 6. Density of states (DOS) and the number of states (NOS) functions as obtained from the bands of Fig. 4. The x-ray photoelectron spectrum (XPS) of Nemoshalenko *et al.*, Ref. 11, is shown for comparison.

TABLE III. Density of states at the Fermi level $N(E_F)$ and the derived specific-electronic-heat capacity γ_{th} for several band models. The calculated heat capacity is compared with the measured value, Ref. 5, to obtain an average mass enhancement. The column marked NR corresponds to a completely nonrelativistic calculation while the column marked −sp-o has the mass-velocity and Darwin corrections but not the spin-orbit interaction included. The column marked + sp-o has also the spin-orbit interaction included, and gives the $N(E_F)$ that may be read off Fig. 6.

	Cu_4	$AuCu_3$ NR	$AuCu_3$ −sp-o	$AuCu_3$ +sp-o
$N(E_F)$ (electrons/cell Ry	15.4	12.3	13.9	14.0
γ_{th} (mJ/K^2 mole)	2.67	2.14	2.40	2.43
γ_{exp} (mJ/K^2 mole)		2.61		
γ_{exp}/γ_{th}		1.22	1.09	1.07

tions give the highest state density, is in accordance with the picture given in Fig. 5, where the Au 6*s* band sinks down towards the Fermi level as a result of the mass-velocity and Darwin corrections [see panels (e) and (a)]. The table also lists the calculated electronic heat capacity and the derived many-body enhancement.

B. Fermi surface

The Fermi surface obtained from the bands of Fig. 4 is shown in Fig. 7. It has one closed hole sheet from band 22 centered at Γ, and one closed electronsheet from band 24 centered at the corner *R* of the Brillouin zone. Finally, it has a multiply connected sheet which takes on the form of a network of tubes with the axis along the edges of the zone. Unfortunately the formation of antiphase domains in samples of pure $AuCu_3$ seems to prevent measurements of the de Haas–van Alphen effect in ordered $AuCu_3$, and there is at present no experimental evidence for the Fermi surface proposed in Fig. 7.

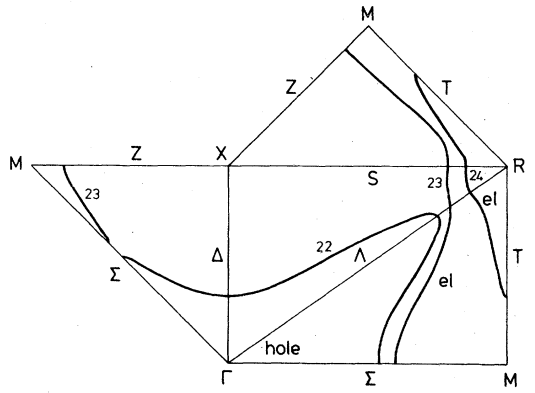

FIG. 7. Fermi surface of ordered $AuCu_3$ as obtained from the band structure in Fig. 4.

VI. OPTICAL PROPERTIES

In this section we present the calculated joint density of states $J(\omega)$ as derived from the relativistic band structure, and compare with the measured spectra. We further show band-to-band decompositions of $J(\omega)$ in the form of partial joint density of states functions $J_{ij}(\omega)$, each giving the density of vertical transitions from that part of band *i* which is below the Fermi level to that part of band *j* which is above the Fermi level. In order to see if it is possible to obtain a different set of interpretations of the experimental spectra we also mention results from other band models, e.g., nonrelativistic bands and bands of fcc copper folded into the simple cubic Brillouin zone (in our terminology Cu_4).

A. Calculated spectra above the edge

In Fig. 8 we show $J(\omega)/\omega$ and some selected partial joint density of states functions $J_{ij}(\omega)$ obtained from the energy bands of Fig. 4. The most prominent structure in the calculated spectrum is seen to be the sharp edge at 2 eV, which is similar to the interband absorption edge in pure copper.[19] In contrast to the case of copper however, we notice that owing to the lower symmetry of $AuCu_3$, there are interband transitions below the edge down to an energy of the order of the spin-orbit splitting of the Λ_3 level.

The edge is found to have transitions from the top of the Cu 3*d* band to the Fermi surface in bands

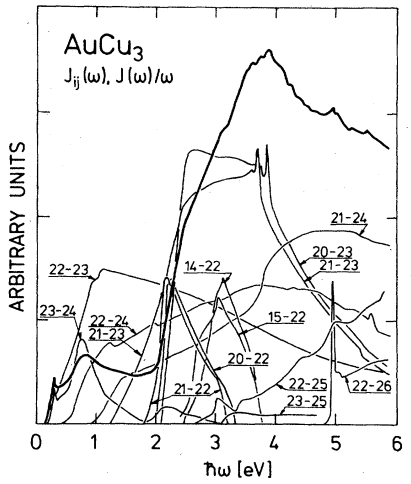

FIG. 8. Joint density of states divided by ω (heavy line) and several selected partial joint density of states function (thin lines). The results are obtained from the energy bands of Fig. 4.

22 and 23, exemplified in Fig. 8 by $J_{20,22}(\omega)$ and $J_{20,23}(\omega)$, respectively. Note that there is a whole series of J_{ij}'s of almost the same shape as $J_{20,22}$ and $J_{20,23}$, but moving gradually towards higher energies as the initial state is taken from farther below in the Cu $3d$ band.

The transitions involving band 22 are bound in k space by the Fermi surface sheet centered at Γ, and they first occur at Δ for $J_{21,22}$, and at Λ for $J_{20,22}$ and the similar functions. As the photon energy is increased the region of transitions to band 22 shrinks and the contributions disappear when Γ is reached. The transitions to band 23 ($i<21$) set in at Λ, give rise to the first maximum in $J_{i,23}$ along a line parallel to T and to the second maximum when the critical points at Δ and Γ are reached. These transitions near Γ are equivalent to the transitions at X close to 4 eV in pure copper.

If we compare the edge in $J(\omega)/\omega^2$ of Fig. 8 with the nonrelativistic and the Cu_4 calculations we find that the Cu_4 results coincide with the relativistic calculation, while the nonrelativistic calculation places the edge at 3 eV. The latter result is similar to the calculations for pure gold,[25] and is consistent with the fact that the Cu $3d$ and the Au $5d$ bands coincide in the nonrelativistic case [see Figs. 5(d) and 5(e)].

Turning again to $J(\omega)/\omega$, we find at 3 eV a shoulder caused by the superposition of transitions from a sub-d band (see, for instance, $J_{14,22}$) to band 22 and the d-band to band-23 transitions. Finally, in the range above the edge we find a maximum at 5 eV originating in transitions from band 22 to bands 26 and 27 at R, and in transitions from the top of the Au $5d$ band to the Fermi level.

B. Calculated spectra below the edge

Almost all the transitions contributing to the optical interband absorption in the infrared, i.e., below the edge at 2 eV have their origin in the energy bands close to the symmetry line T. It is seen from Fig. 4 that there are three possible critical points at M, of which however M_6^+-M_7^+ is forbidden by selection rules. If we move along Z or S we find that bands 23 and 24 become almost parallel, leading to possibly large contributions to the joint density of states. If we furthermore move away from T but plot the bands along lines parallel to T we find that bands 21–24 are almost horizontal over a distance in reciprocal space of half the MR distance, again resulting in possibly large contributions to $J(\omega)$.

The partial joint density of states function $J_{23,24}$ has a maximum at 0.3 eV originating in transitions on a line parallel to T. The transitions start along S and move with increasing photon energy towards Z, where they disappear. The second maximum at 0.8 eV originates in transitions close to the M_7^-, M_7^+ critical point in the large region of nearly horizontal bands mentioned above.

The transitions responsible for $J_{22,23}$ start simultaneously at the Fermi level along Σ and Λ, respectively, and give rise to a maximum at 1.1 eV when they reach Z and S. The transitions leading to $J_{22,24}$ start at Λ, move to the critical point M_6^+, M_7^+, where they are forbidden by selection rules, and they develop a small maximum when the region of horizontal bands close to T is reached. The remaining partial joint density $J_{21,24}$ is in the range below 2 eV due to transitions starting at the M_6^-, M_7^+ critical point, and moving rapidly out in the zone as the photon energy is increased.

If we compare in the range below the edge $J(\omega)/\omega^2$ from several band models we find that the result from the Cu_4 calculation is almost featureless in the infrared, while the two $AuCu_3$ models both predict two peaks in this energy range. In the nonrelativistic calculation the peaks have moved to higher photon energies (they are now at 0.6 and 1.4 eV) reflecting the larger band splittings at M [see Figs. 6(b) and (d)] and along S. Since band 23 is close to band 24 and the Fermi level in the nonrelativistic case the origin of the second peak is in transition from band 22 to 23, as opposed to 23 to 24 for the relativistic calculation.

C. Comparison with experiments

We have now described the origin of the structural elements in the calculated spectra and are in a position to compare with the experimental observations. However, before we actually make this comparison, a few remarks concerning the accuracy of both the experimental and the calculated interband spectra are in order.

The intraband correction employed, Eq. (1) is of the simplest possible form. It is well known and also easily seen from Fig. 3 that the form and the position of structure in the corrected experimental spectrum is sensitive to the choice of A and B. The correction [Eq. (1)] is therefore used only to bring out structure in the infrared region.

The calculated spectra are obtained in the constant matrix-element approximation, and accordingly the line shape of these spectra should be regarded with some caution. Because of this and the inaccuracy of the Drude correction, we have taken the viewpoint that in the comparison between theory and experiment agreement in the spectral position of structure is a stronger argument for a given interpretation than is agreement in actual lineshape.

In Fig. 9 the measured imaginary part of the di-

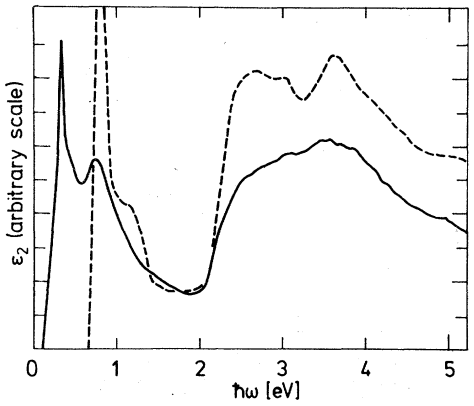

FIG. 9. Comparison between the experimental intraband corrected $\epsilon_2(\omega)$ spectrum and $J(\omega)/\omega^2$ obtained from the relativistic bands of Fig. 4.

electric constant $\epsilon_2(\omega)$ corrected for intraband contributions is compared with $J(\omega)/\omega^2$, $J(\omega)$ being the joint density of states. In view of the above mentioned shortcomings, the overall agreement is satisfactory. It is possible to give an interpretation of all structures observed experimentally in terms of our band structure.

We find that: (a) the main edge at 2 eV (see Fig. 1) is due to transitions from the top of the Cu 3*d* band to bands 22 and 23 at the Fermi level; (b) the contributions to $\epsilon_2(\omega)$ close to 2.5 eV come from transitions between the top of the Cu 3*d* band and conduction states in band 23 on a line parallel to T; (c) the minute peak at 3 eV is due to transitions from a Cu sub-*d* band to conduction states approximately halfway between Γ and the Fermi surface in band 22; (d) the main contributions to the pronounced peak at 3.6 eV come from transitions from the top of the Cu 3*d* band to band 23 close to Γ; and (e) the maximum at 5 eV is due to transitions from the top of the Au 5*d* band to the Fermi level and to transitions at the R_7^-, R_8^+ critical point.

In the infrared the peak at 0.8 eV has its origin in transitions at and close to the M_7^-, M_7^+ critical point, and the shoulder at 1.2 eV may originate in transitions from band 22 to either band 23 or 24 (see Fig. 9) in a region close to T. If we compare the experimental spectra with the nonrelativistic $J(\omega)/\omega^2$ we may obtain a different interpretation of the structure in the infrared as discussed in Sec. VI. B. However, this would require changes in the band structure of the order of 0.2 eV, and although this may be possible, we find that the interpretation given above is at present the most plausible.

The agreement in the position of the edge at 2.0 eV shows together with the photoemission results, and the x-ray photoelectron spectrum Fig. 6, that the Cu 3*d* band is positioned correctly in the present relativistic calculation. This is very satisfactory, since the position of *d* bands is sensitive to the crystal potential chosen, and shows that the present choice is a reasonable one.

D. Disordered $AuCu_3$

When the $AuCu_3$ alloy is disordered, the electronic specific heat[4,5] is increased by 4%, the optical absorption spectrum[7,8] is virtually unchanged above the edge except for a 10% reduction close to 3.6 eV that removes the peak at this spectral position, the diamagnetic susceptibility[26] is decreased by 15%, and a shoulder disappears in the x-ray photoelectron spectrum.[11] This leads to the conclusion that, although the changes are significant they are *small*, and thus the disordered alloy is well described to a first approximation by the electronic structure of the ordered compound.

Even though a change of 10% in the optical absorption is beyond the accuracy of the present calculation, we may still, in the light of our band calculation, discuss the suggestions[7,8,10,27] put forward to explain the behavior with ordering of the peak at 3.6 eV in the $\epsilon_2(\omega)$ spectrum.

Nilsson and Norris[8] suggested that energy gaps caused by new Bragg planes may be responsible for the appearance of the extra peak in the ordered phase. We do find such gaps on the (100) *MXR* plane as seen from Figs. 4 and 5. However, these gaps are responsible for the optical properties in the infrared and not for the absorption at 3.6 eV.

The plane that causes the gaps along S, T, and Z also transforms X of the fcc zone into Γ of the sc zone, resulting in new transitions. One particular example is the Δ_6-Δ_6 transition from the Fermi surface in band 22, and since this occurs at 3.3 eV in the calculation by Gray and Brown,[12] Stahl *et al.*[7] suggested that this transition was responsible for the 3.6-eV peak. In the present case however, the transition from band 22 to band 23 appears along Δ at 2.5 eV, and does not give rise to any particular feature in the $J_{22,23}(\omega)$ function shown in Fig. 8. Thus neither of the two above mentioned suggestions are substantiated by the present calculations.

The explanation offered by Winsemius *et al.*[27] is based on the observation that, although the absorption in the noble metals to a large degree is determined by transitions from the *d* bands, interconduction-band transitions play an important role in shaping the spectrum. Since interconduction-band transitions are more sensitive to internal strain than *d*-band transitions the former will be smeared out in a poor or disordered sample. Judged from the present results this mechanism could also be at work in $AuCu_3$ and thus account

for the disappearance of the peak at 3.6 eV in the disordered sample.

Scott and Muldawer[10] examined the folding of energy bands into the simple cubic Brillouin zone accompanying the formation of the superlattice in $AuCu_3$. They especially point to new transitions close to M and Γ as a possible source of the change in the optical properties upon ordering. We do indeed find that some of the absorption in the infrared is caused by the critical point at M induced by the (100) Bragg plane. The fact that this contribution disappears in the disordered sample is in accordance with the folding concept. We also find that the new transitions close to Γ contribute to the spectrum near 3.6 eV. The transitions involved are from bands 16, 17, and 18 to band 23 and they give rise to partial joint density functions similar to $J_{21,23}(\omega)$ shown in Fig. 8. However, the joint density of states obtained from an fcc copper calculation (using potential parameters from Table II) where these transitions do not exist, is very similar to $J(\omega)$ for Cu_4, so that the effect of these transitions seems to be small on the scale of the total $J(\omega)$. Without the knowledge of the matrix elements it is therefore very difficult to substantiate the claim that these transitions at Γ are the cause of the change in $\epsilon_2(\omega)$ near 3.6 eV.

VII. CONCLUSION

We have measured the optical properties of the intermetallic compound $AuCu_3$ at low temperatures. The experimental $\epsilon_2(\omega)$ spectrum is found to have an absorption edge at 2 eV similar to the edge in pure copper, and five additional structural elements in the range above the edge. In contrast to the case of pure copper (and gold), there are interband contributions below the edge in the infrared region.

The electronic structure of $AuCu_3$ has been calculated using the relativistic linear muffin-tin orbitals method with a modest computational effect, and with an accuracy similar to that obtainable in calculations on pure elements. The Fermi surface and the state density have been obtained. The comparison with the electronic specific heat capacity suggests an average mass enhancement of 1.1 at the Fermi level. The calculated $\epsilon_2(\omega)$ forms, within the limitations of the constant matrix-element approximation, a reasonable framework for the the interpretation of the optical experiments on $AuCu_3$. It is thus possible to give an interpretation of all the structural elements observed experimentally.

The comparison with the optical measurements, the x-ray photoelectron spectrum, and the photoemission curves show that the calculated Cu 3d band has the correct position, while the Au 5d band seems to be positioned 0.4 eV too low.

Finally, we note that performing optical measurements at very low temperatures is an effective technique for revealing structure in the optical spectra otherwise hidden in the Drude region. In view of the growing interest in ordered compounds, this may be an important observation, since band calculations suggest that many compounds will have interband transitions at low photon energies.

ACKNOWLEDGMENTS

It is a pleasure to thank J. Mydosh, P. Winsemius, P. de Chatel, R. Zweistra, and H. Stocker for their continuous interest in the measurements and their interpretation. One of us (H.L.S.) wants to thank J. Mydosh and the Metal Physics Group at Kammerlingh Onnes Laboratory for their hospitality, and to acknowledge support from Stichting voor Fundamenteel Onderzoek der Materie (FOM).

---

*Present address: Research Establishment Risø, DK-4000 Roskilde, Denmark.

[1]D. Beaglehole and E. Erlbach, Phys. Rev. B 6, 1209 (1972).
[2]P.-O. Nilsson, Phys. Kondens. Mater. 11, 1 (1970).
[3]T. Muto and Y. Takagi, *Solid State Physics*, edited by F. Seitz and D. Turnbull (Academic, New York, 1955), Vol. 1.
[4]D. L. Martin, Can. Phys. 46, 923 (1968).
[5]D. L. Martin, Phys. Rev. B 14, 369 (1976).
[6]W. Köster and R. Stahl, Z. Metallkd. 58, 768 (1967).
[7]R. Stahl, H.-J. Spranger, and H.-P. Aubaus, Z. Metallkd. 60, 933 (1969).
[8]P.-O. Nilsson and C. Norris, Phys. Lett. A 29, 22 (1969).
[9]J. Rivory, J. Phys. (Paris) 35, C 4-51 (1974).
[10]W. Scott and L. Muldawer, Phys. Rev. B 9, 1115 (1974).
[11]V. V. Nemoshkalenko, K. V. Chuistov, V. G. Aleshin, and A. I. Senkevich, J. Electron Spectros. 9, 169 (1976).
[12]D. Gray and E. Brown, Phys. Rev. 160, 567 (1967).
[13]O. K. Andersen, Phys. Rev. B 12, 3060 (1975).
[14]O. K. Andersen, Solid State Commun. 13, 133 (1973).
[15]H. L. Skriver, Phys. Rev. B 14, 5187 (1976).
[16]H. L. Skriver, Phys. Rev. B 15, 1894 (1977).
[17]H. L. Skriver and N. E. Christensen, Phys. Rev. B 8, 3778 (1973); H. L. Skriver, Phys. Status Solidi B 58, 721 (1973).
[18]O. Jepsen and O. K. Andersen, Solid State Commun. 9, 1763 (1971).
[19]J. F. Janak, A. R. Williams, and V. L. Moruzzi, Phys. Rev. B 11, 1522 (1975).
[20]A. W. A. v. d. Hart (private communication).

[21]D. H. Seib and W. E. Spicer, Phys. Rev. B 2, 1676 (1970).
[22]P. Winsemius, thesis (University of Leiden, 1973) (unpublished).
[23]P. Winsemius, F. F. van Kampen, H. P. Lengkeek, and C. G. van Went, J. Phys. F 6, 1583 (1976).
[24]A. P. Lenham, J. Ost. Soc. Am. 57, 473 (1967).
[25]N. E. Christensen and B. O. Seraphin, Phys. Rev. B 4, 3321 (1971).
[26]H. J. Seemann and E. Vogt, Ann. Phys. N.Y. 2, 976 (1929).
[27]P. Winsemius, H. P. Lengkeek, and F. F. van Kampen, Physica (Utr.) 79 B, 529 (1975).